Lu et al. Nanoscale Research Letters (2015) 10:385
DOI 10.1186/s11671-015-1092-z

Nanoscale Research Letters
a SpringerOpen Journal

NANO EXPRESS Open Access

Synthesis of $BiPO_4/Bi_2S_3$ Heterojunction with Enhanced Photocatalytic Activity under Visible-Light Irradiation

Mengna Lu, Guotao Yuan, Zuoshan Wang*, Yuyuan Wang and Jun Guo

Abstract

$BiPO_4/Bi_2S_3$ photocatalysts were successfully synthesized by a simple two-step hydrothermal process, which involved the initial formation of $BiPO_4$ rod and then the attachment of Bi_2S_3 through ion exchange. The as-synthesized products were characterized by X-ray diffraction (XRD), scanning electron microscope (SEM), transmission electron microscopy (TEM), X-ray photoelectron spectroscopy (XPS), and UV-vis diffuse reflectance spectra (UV-vis DRS). It was found that $BiPO_4$ was regular rods with smooth surfaces. However, $BiPO_4/Bi_2S_3$ heterojunction had a rough surface, which could be attributed to the attachment of Bi_2S_3 on the surface of $BiPO_4$ rods. The $BiPO_4/Bi_2S_3$ composite exhibited better photocatalytic performance than that of pure $BiPO_4$ and Bi_2S_3 for the degradation of methylene blue (MB) and Rhodamine B (RhB) under visible light. The enhanced photocatalytic performance could be ascribed to synergistic effect of $BiPO_4/Bi_2S_3$ heterojunction, in which the attached Bi_2S_3 nanoparticles could improve visible-light absorption and the $BiPO_4/Bi_2S_3$ heterojunction suppressed the recombination of photogenerated electron-hole pairs. Our work suggested that $BiPO_4/Bi_2S_3$ heterojunction could be a potential photocatalyst under visible light.

Keywords: $BiPO_4/Bi_2S_3$; Photocatalytic activity; Hydrothermal method; Heterojunction photocatalyst

Background

Currently, semiconductor photocatalysts have attracted a lot of interests due to their widely applications for the degradation of organic contaminants [1–4] and generation of hydrogen from water [5]. Generally speaking, a highly efficient photocatalyst must have a wide photoabsorption range, as well as the low recombination rate of photogenerated electron-hole pairs. Therefore, it is also a challenge to develop a new compound with high photocatalytic efficiency under visible light [6–9].

As a potential photocatalyst, $BiPO_4$ has recently been extensively studied [10–12]. It has been reported that the photocatalytic activity of $BiPO_4$ is strongly dependent on its crystal structure [13] and the monoclinic phase $BiPO_4$ showed a better photocatalytic performance than that of P25 for the photodegradation of organic contaminants under UV irradiation [14]. However, $BiPO_4$ had a wide band gap of about 3.8 eV and thus can only be excited by UV light to generate electron-hole pairs [11]. In order to improve the visible-light utilization of $BiPO_4$, many efforts have been taken. Lin et al. fabricated $Ag_3PO_4/BiPO_4$ heterojunction with enhanced photocatalytic ability under visible-light irradiation [15]. Duo et al. reported that $BiPO_4/BiOCl$ heterojunction also had enhanced photocatalytic activity [16]. Li et al. found that $BiPO_4/g\text{-}C_3N_4$ heterojunction could efficiently respond to visible-light irradiation [17]. Besides, Zhang et al. reported that $BiPO_4$/reduced graphene oxide composites with specific surface areas had better photocatalytic activity for the degradation of MB [18]. Whereas, coupling of $BiPO_4$ with other semiconductors is still meaningful for improving light absorption in the visible spectrum and suppressing the recombination of the photogenerated electron-hole pairs more effectively.

Bi_2S_3, a small band gap semiconductor (1.3 eV), has a high photoabsorption coefficient [19–21]. Hence, it can usually be used as a potential visible-light photocatalyst through combination from other semiconductors to improve light absorption and separation efficiency of

* Correspondence: zuoshanwang@suda.edu.cn
College of Chemistry, Chemical Engineering and Materials Science, Soochow University, Soochow 215123, China

photogenerated electron-hole pairs, such as CdS/Bi_2S_3 [22], $BiVO_4/Bi_2S_3$ [23], Bi_2S_3/BiOBr [24], and so on.

In this study, we reported the preparation of a novel $BiPO_4/Bi_2S_3$ heterostructure and their photocatalytic properties were evaluated by the degradation of MB and RhB under visible light. As expected, the as-prepared $BiPO_4/Bi_2S_3$ heterojunction exhibited enhanced visible-light photocatalytic activity and a possible mechanism was presented.

Methods

Materials and Preparation

All reagents were of analytical purity (Sinopharm Chemical reagent Co., Ltd., China) and used without further purification.

Synthesis of $BiPO_4$

$BiPO_4$ was prepared by a facile hydrothermal method. Firstly, 0.5 g of PVP was dissolved in a beaker with deionized water (50 mL) under stirring. Secondly, $Bi(NO_3)_3 \cdot 5H_2O$ and $NaH_2PO_4 \cdot 12H_2O$ (molar radio of 1:1) were added into the solution. After the pH of the reaction system was adjusted to 3 by HNO_3, the solution was transferred into a 100-mL Teflon-lined stainless steel autoclave and heated at 180 °C for 24 h. When the system cooled down to room temperature naturally, the resulting product was harvested and washed with deionized water and absolute alcohol for several times. Finally, the as-prepared products were dried at 60 °C for 12 h.

Synthesis of $BiPO_4/Bi_2S_3$ Photocatalyst

The $BiPO_4/Bi_2S_3$ photocatalyst was prepared through an in situ ion exchange process. Typically, 0.1 g of PVP was dissolved in 50 mL of ethylene glycol, followed by the addition of 0.456 g of $BiPO_4$ under stirring to achieve suspension. Then, a certain amount of thiourea (the amount of thiourea was 0.086, 0.172, and 0.573 g, and they are named as BB-1, BB-2, and BB-3, respectively.) was added into above suspension and the solution was transferred into a 100-mL Teflon-lined stainless steel autoclave, which was sealed and maintained at 140 °C for 3 h. After the autoclave was cooled to room temperature naturally, the precipitates were collected and washed with water and ethanol several times. The $BiPO_4/Bi_2S_3$ products were dried at 60 °C for 12 h. For comparison, pure Bi_2S_3 was prepared through hydrothermal method according to the literature [25].

Characterization of the As-prepared Samples

The phase of the samples was measured by XRD (D/Max-ⅢC, Shimadzu) using an X-ray diffractometer with Cu Kα radiation. The morphology was analyzed by SEM on Hitachi S-4600 and TEM (FEI Tecnai G20). UV-vis DRS was tested on a Shimadzu UV240 UV-vis spectrophotometer with $BaSO_4$ as a reference material. The elemental composition of the samples was analyzed by X-ray photoelectron spectrometer (XPS, USA Thermo ESCALAB 250).

Photocatalytic Activity

The photocatalytic performance of $BiPO_4/Bi_2S_3$ heterojunction photocatalyst was evaluated by the degradation of MB and RhB under visible light. In each experiment, 50 mg of different photocatalysts were added into 100 mL of MB or RhB solution (10 mg/L) in a reactor. Before irradiation, the mixture was magnetically stirred for 30 min in the dark to achieve the adsorption/desorption equilibrium between dye and photocatalysts. Then, the solution was irradiated by visible light under continuous stirring. At a defined time interval, about 3 mL of solution was extracted from the reactors and then centrifuged to remove catalysts before analysis. Finally, MB (RhB) solution was analyzed through a UV-vis spectrophotometer. The degradation rate could be obtained through the formula [26]: $\eta = C_i/C_0 \times 100$ %, where C_i was the absorbance of MB (RhB) which was measured every 30 min, and C_0 was the absorbance of MB (RhB) before light up.

Results and Discussion

Phase and Crystal Structure Analysis

Figure 1 shows the XRD patterns of $BiPO_4$ and $BiPO_4/Bi_2S_3$ heterojunction with different Bi_2S_3 contents. In the pure $BiPO_4$, all the diffraction peaks are well matched with the monoclinic phase of $BiPO_4$ (JCPDS File No. 89–0287), indicating that the as-prepared $BiPO_4$ has the high purity. On the other hand, the $BiPO_4/Bi_2S_3$ composites exhibit a mixture of two crystalline phases. One can be identified as $BiPO_4$, and the others originate from rutile Bi_2S_3 [25]. Furthermore, the intensities

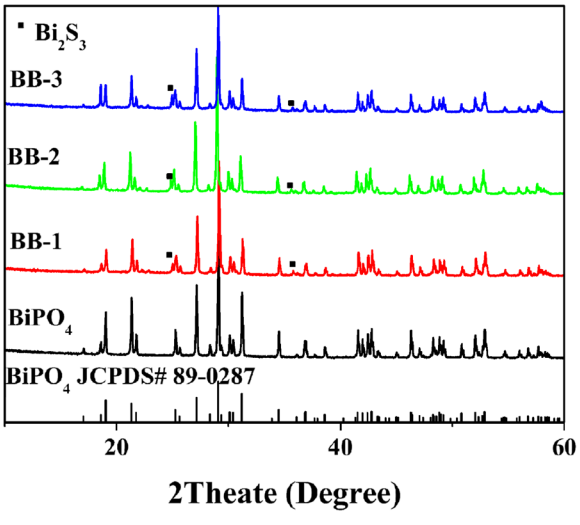

Fig. 1 XRD patterns of different as-prepared samples

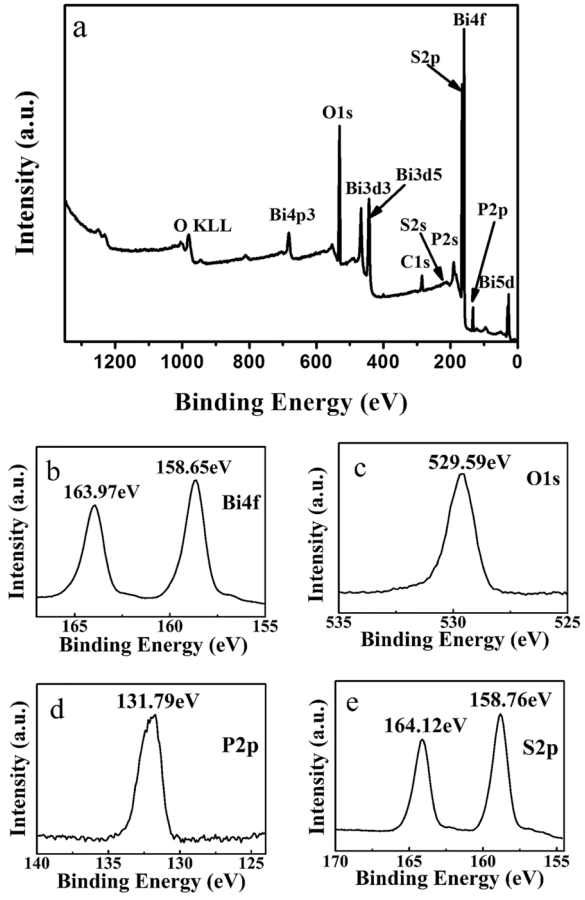

Fig. 2 The XPS survey spectra of BB-2 (**a**) and high-resolution XPS spectra of Bi 4f (**b**), O 1 s (**c**), P 2p (**d**) and S 2p (**e**)

of corresponding to diffraction peaks of Bi_2S_3 gradually strengthen along with the increase of the Bi_2S_3 content, while those of $BiPO_4$ simultaneously weaken. No other characteristic peaks of impurity are detected, suggesting that $BiPO_4/Bi_2S_3$ composites are only composed of $BiPO_4$ and Bi_2S_3 phases.

The surface chemical composition of BB-2 is analyzed by XPS and the results are shown in Fig. 2. The XPS survey spectrum (Fig. 2a) shows that BB-2 contains Bi, P, S, and O elements, which is consistent to XRD results. Besides, C 1 s peak is also seen in XPS survey spectrum, which can be attributed to adventitious hydrocarbon from instrument. Two peaks appear at 163.97 and 158.65 eV in Fig. 2b, which are corresponding to Bi $4f_{5/2}$ and Bi $4f_{7/2}$ peaks of Bi^{3+}, respectively [27]. In Fig. 2c, O 1 s peak appeared at 529.59 eV, in which it can be attributed to lattice oxygen in crystalline $BiPO_4$ [28]. In Fig. 2d, the P 2p XPS peak appeared at 131.79 eV, suggesting that P exists in the oxidation of P^{5+}. On the other hand, the binding energies of 164.12 and 158.76 eV are attributed to S 2p peaks (Fig. 2e), which prove the existence of S^{2-} [29].

Morphology Analysis

Figure 3 shows the SEM images of $BiPO_4$ and $BiPO_4/Bi_2S_3$ composites. It can be seen from Fig. 3a that pure $BiPO_4$ shows regular rod shape with diameter of 200–400 nm and the length of 500–2000 nm. It should be noted that these rods have smooth surfaces. Figure 3b–d shows the SEM images of different $BiPO_4/Bi_2S_3$ composites. Compared with pure $BiPO_4$, the surfaces of $BiPO_4/Bi_2S_3$ composites become rough. Furthermore, with the increasing amount of additive thiourea, more Bi_2S_3 nanoparticles can be observed on the surface of $BiPO_4$ rods gradually, which is also consistent to XRD results.

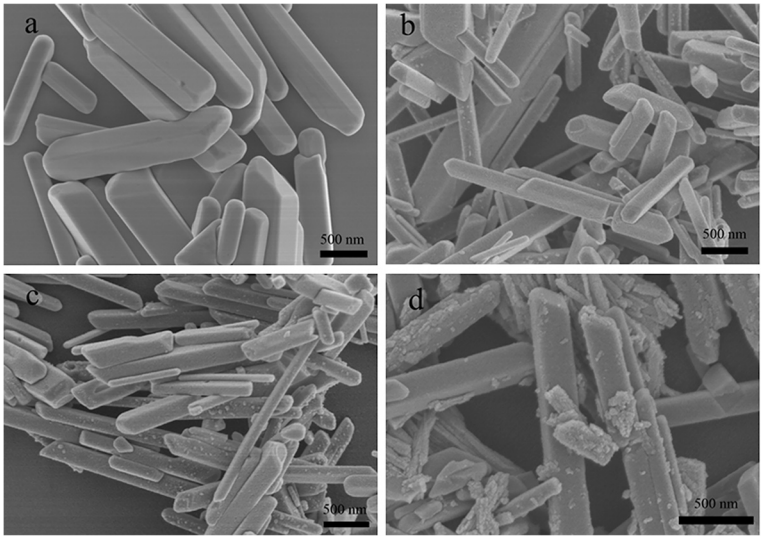

Fig. 3 SEM images of pure $BiPO_4$ (**a**), BB-1 (**b**), BB-2 (**c**) and BB-3 (**d**)

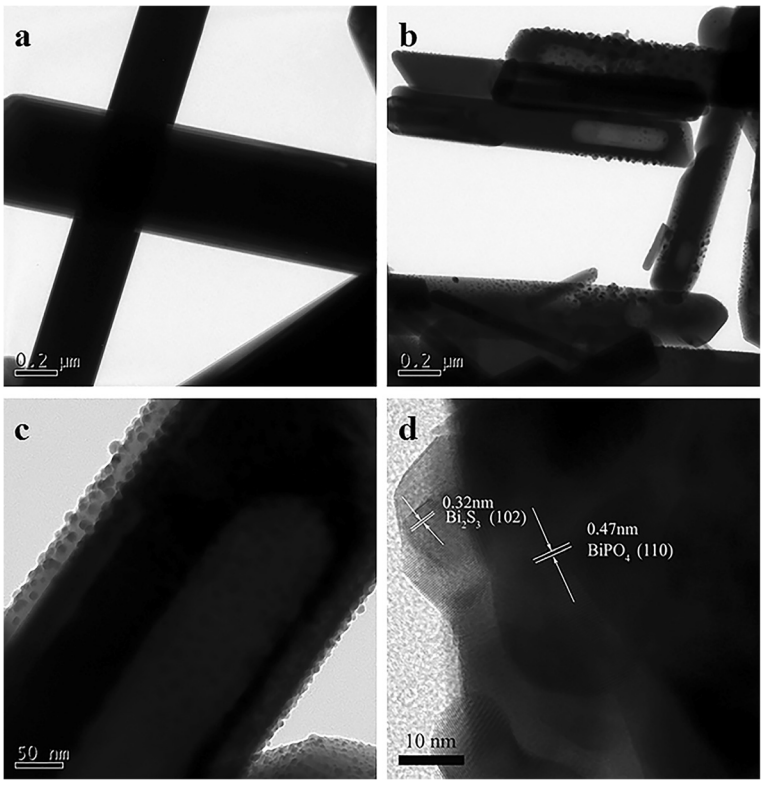

Fig. 4 TEM images of $BiPO_4$ (**a**), BB-2 (**b**, **c**), and HRTEM image of BB-2 (**d**)

TEM and HRTEM images are shown in Fig. 4, which display identified results as those of SEM analysis. From Fig. 4a, one can see that pure $BiPO_4$ are regular rods with a smooth surface. While $BiPO_4/Bi_2S_3$ heterojunction shows a rough surface, suggesting the successful attachment of Bi_2S_3 on the surface of $BiPO_4$ rods. Furthermore, the lattice spacings can be clearly seen in the corresponding HRTEM image (Fig. 4d). The fringe spacing of 0.47 nm is indexed to the (1 1 0) lattice plane of monoclinic $BiPO_4$, while 0.32 nm is agreed with the (1 0 2) lattice plane of Bi_2S_3. Therefore, it can be summarized that $BiPO_4/Bi_2S_3$ heterojunction is achieved through a facile ion-exchange method.

UV-vis Analysis

Figure 5a shows UV-vis DRS of as-prepared $BiPO_4$, Bi_2S_3, and $BiPO_4/Bi_2S_3$ composites. It reveals that $BiPO_4/Bi_2S_3$ composites have a stronger absorption than that of $BiPO_4$ in visible light. The band gap energy can be achieved through the formula [30, 31]. Besides, according to the literature, n values of $BiPO_4$ and Bi_2S_3 are 4 [32] and 1 [33], respectively. Therefore, as is shown in Fig. 5b, E_g

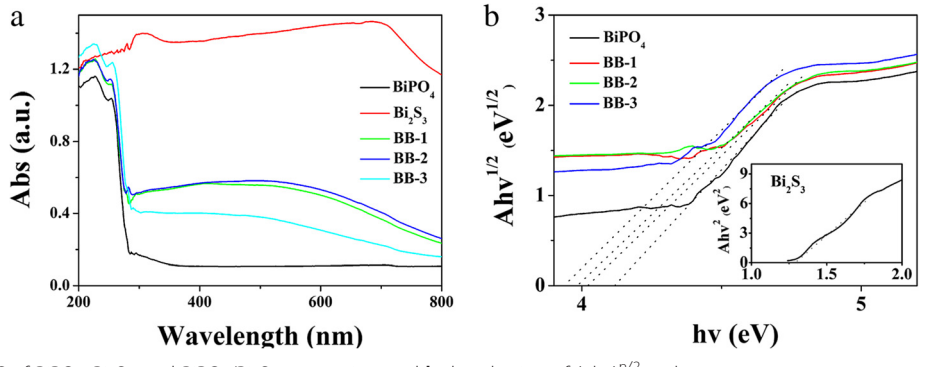

Fig. 5 a UV-vis DRS of $BiPO_4$, Bi_2S_3, and $BiPO_4/Bi_2S_3$ composites and **b** the plotting of $(\alpha hv)^{n/2}$ vs. hv

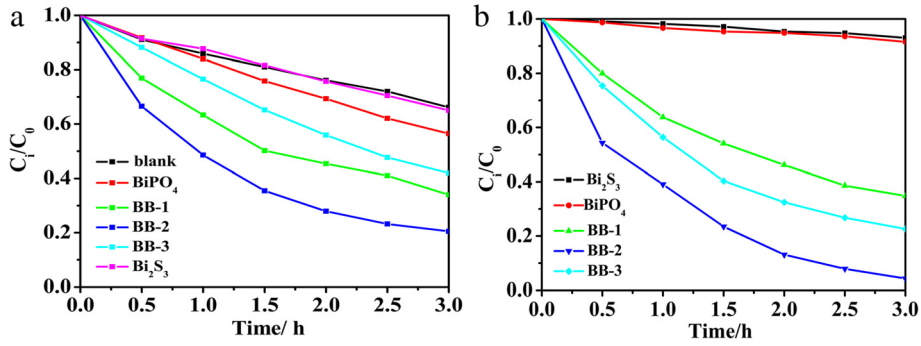

Fig. 6 a Photodegradation rate of MB under visible-light irradiation with different samples, **b** photodegradation rate of RhB under visible-light irradiation with different samples

of $BiPO_4$ and Bi_2S_3 can be calculated as 4.08 and 1.30 eV. Moreover, E_g of BB-1, BB-2, and BB-3 are 4.01, 3.93, and 3.81 eV, respectively. Besides, Bi_2S_3 displays quantum size effect, which may influence the band gap, the position of both CB and VB band. Besides, the band gap shift relative to the bulk can be calculated by the following formula [34, 35]:

$$\Delta E_g(R) = \frac{h^2}{8m_oR^2}\left(\frac{1}{m_e^*} + \frac{1}{m_h^*}\right),$$

in which ΔE_g (R) is the band gap shift, h is the Planck's constant, and R is the crystal radius. Besides, m_o is electron mass and m_e^* and m_h^* are the effective masses of electrons and holes, respectively. Then, the size of Bi_2S_3 nanoparticles attached on the surface of $BiPO_4$ rods can be calculated as 2.68, 2.72, and 2.78 nm, respectively, which is much smaller than Bohr excitation radius of 24 nm. Therefore, quantum size confinement can be observed obviously, which influences the band gap, the position of both CB and VB band, etc. These results also support the enhancement of photocatalytic activity.

Photocatalytic Activity of Different Samples

The photocatalytic performance of $BiPO_4/Bi_2S_3$ heterojunction was assessed by photodegradation of MB under visible-light irradiation (Fig. 6a). It can be seen that pure $BiPO_4$ shows poor photocatalytic ability in degrading MB (40 %). Interestingly, the coupling of $BiPO_4$ with Bi_2S_3 leads to notable enhancement MB photodegradation. The MB removal rates are about 50, 80, and 60 %, respectively. Meantime, RhB here is also employed as an organic pollutant to further confirm the photodegradation activity of $BiPO_4/Bi_2S_3$ heterojunction. As shown in

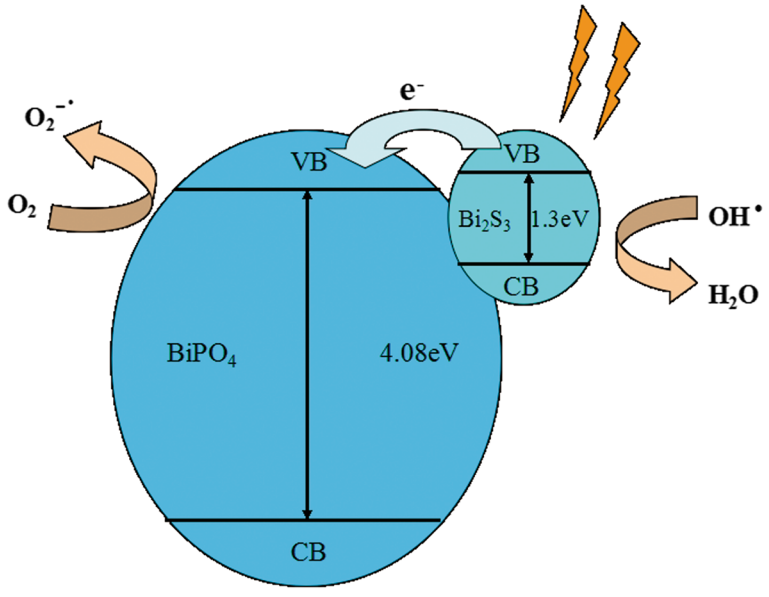

Fig. 7 Schematic illustration of possible electrons and hole transfer mechanism of $BiPO_4/Bi_2S_3$ heterostructure

Fig. 6b, $BiPO_4/Bi_2S_3$ composites show better photocatalytic activity in the degradation of RhB than that of pure $BiPO_4$ and the best photocatalytic property was achieved for BB-2 sample. The enhanced visible-light-driven activity of the heterostructure must be attributed to the synergistic effect between $BiPO_4$ and Bi_2S_3. What is more, the quantum size confinement of Bi_2S_3 in the visible spectrum also leads to the enhancement of photocatalytic activity. However, the excess Bi_2S_3 content in $BiPO_4/Bi_2S_3$ composite will cause their photocatalytic performance to decrease (BB-3). It may be attributed to these reasons: one is reduction of active sites due to the excess Bi_2S_3 nanoparticles on the surface $BiPO_4$ rod [36]. The other is that excessive narrow band gap Bi_2S_3 may lower the separation efficiency of electron-hole pairs and further inhibit the photocatalytic activity [37].

Possible Photocatalytic Mechanism

The band positions of $BiPO_4$ and Bi_2S_3 are evaluated based on the equation [38]. Hence, the valence band and conduction band edge potential (E_{VB} and E_{CB}) of $BiPO_4$ and Bi_2S_3 are 4.39 eV, 0.31 eV and 1.43 eV, 0.13 eV, respectively. Therefore, the possible mechanism is shown in Fig. 7. Bi_2S_3 nanoparticles absorb the visible light and give rise to electron-hole pairs. The photo-excited electrons in Bi_2S_3 CB will transfer to $BiPO_4$ rods and holes are left in Bi_2S_3 VB, which will decrease recombination rate of photogenerated charge carriers. The electrons in $BiPO_4$ CB can rapidly adsorb O_2 to form $O_2^{-\bullet}$, while the holes can interact with the absorbed H_2O to achieve hydroxyl radicals. After then, $O_2^{-\bullet}$ and OH• with strong oxidizability can decompose MB (RhB) to generate CO_2 and H_2O. Moreover, $BiPO_4/Bi_2S_3$ heterojunction photocatalysts have a stronger and wider absorption in visible light, which is beneficial to photocatalytic activity.

Conclusions

In summary, we have synthesized the $BiPO_4/Bi_2S_3$ heterojunction with a facile two-step hydrothermal method. Bi_2S_3 nanoparticles can be in situ formed on the surface of $BiPO_4$ rods through ion exchange. As the quantum size confinement of Bi_2S_3 in the visible spectrum, it can be used as photosensitizer. When $BiPO_4$ rods are modified with Bi_2S_3, the separation of electron-hole pairs could be accelerated and the photoabsorption could be promoted as well. These directly led to the enhancement of photocatalytic activity for the degradation of MB (RhB) under visible-light irradiation, and BB-2 sample exhibits the best photocatalytic property. Degradation rate of MB under visible-light irradiation with BB-2 could reach to 80 % in 3 h, double that of pure $BiPO_4$. Besides, degradation rate of RhB could reach to 99.6 % in 3 h, while it only degraded for 8 % by pure $BiPO_4$.

Competing interests

The authors declare that they have no competing interests.

Authors' contributions

The experiments were guided by ML and GY in this work and all the processes were designed by ZW. JG tested and analyzed the dates. YW participated in the discussion and gave useful suggestions. The manuscript was composed by ML. All authors read and approved the final manuscript.

Acknowledgements

The authors are grateful for the financial support of a project funded by the Priority Academic Program Development of Jiangsu Higher Education Institutions and a key project for Industry-Academia-Research in Jiangsu province (BY2013030-04). This study is also supported by Testing and Analysis Center Soochow University.

Received: 14 July 2015 Accepted: 27 September 2015
Published online: 05 October 2015

References

1. Wetchakun N, Chainet S, PhaniChphant S, Wetchakun K (2015) Efficient photocatalytic degradation of methylene blue over $BiVO_4/TiO_2$ nanocomposites. Ceram Int 41:5999–6004
2. Zhou XF, Lu J, Jiang JJ, Li XB, Lu MN, Yuan GT, Wang ZS, Zheng M, Seo HJ (2014) Simple fabrication of N-doped mesoporous TiO_2 nanorods with the enhanced visible light photocatalytic activity. Nanoscale Res Lett 9:34
3. Liu YM, Liu JZ, Lin YL, Zhang YF, Wei Y (2009) Simple fabrication and photocatalytic activity of S-doped TiO_2 under lower power LED visible light irradiation. Ceram Int 35:3061–3065
4. Chen YZ, Zeng DQ, Zhang K, Lu AL, Wang LS, Peng DL (2014) Au-ZnO hybrid nanomultipods and nanopyramids: one-pot reaction synthesis and photocatalytic properties. Nanoscale 6:874–881
5. Abe R, Sayama K, Sugihara H (2005) Development of new photocatalytic water splitting into H_2 and O_2 using two different semiconductor photocatalysts and a shuttle redox mediator IO_3^-/I^-. J Phys Chem B 109:16052–16061
6. Zou ZG, Ye JH, Sayama K, Arakawa H (2001) Direct-splitting of water under visible light irradiation with an oxide semiconductor photocatalyst. Nature 414:625–627
7. Xia JX, Yin S, Li HM, Xu H, Xu YG (2011) Improved visible light photocatalytic activity of sphere-like BiOBr hollow and porous structures synthesized via a reactable ionic liquid. Dalton Trans 40:5249–5258
8. Ismail AA, Bahnemann DW (2011) Mesostructured Pt/TiO_2 nanocomposites as highly active photocatalysts for the photooxidation of dichloroacetic acid. J Phys Chem C 115:5784–5791
9. Fageria P, Gangopadhyay S, Pande S (2014) Synthesis of ZnO/Au and ZnO/Ag nanoparticles and their photocatalytic application using UV and visible light. RSC Adv 4:24962–24972
10. Zhang YA, Fan HQ, Li MM, Tian HL (2013) $Ag/BiPO_4$ heterostructures: synthesis, characterization and their enhanced photocatalytic properties. Dalton Trans 42:13172–13178
11. Xu H, Xu YG, Li HM, Xia JX, Xiong J, Yin S, Huang CJ, Wan HL (2012) Synthesis, characterization and photocatalytic property of $AgBr/BiPO_4$ heterojunction. Dalton Trans 41:3387–3394
12. Lv HW, Shen XP, Ji ZY, Qiu DZ, Zhu GX, Bi YL (2013) Synthesis of graphene oxide-$BiPO_4$ composites with enhanced photocatalytic properties. Appl Surf Sci 284:308–314
13. Pan CS, Zhu YF (2015) A review of $BiPO_4$, a highly efficient oxyacid-type photocatalyst, used for environmental applications. Catal Sci Technol 5:3071–3083
14. Pan CS, Zhu YF (2010) New type of $BiPO_4$ oxy-acid salt photocatalyst with high photocatalytic activity on degradation of dye. Environ Sci Technol 44:5570–5574
15. Lin HL, Ye HF, Xu BY, Cao J, Chen SF (2013) Ag_3PO_4 quantum dot sensitized $BiPO_4$: A novel p-n junction $Ag_3PO_4/BiPO_4$ with enhanced visible-light photocatalytic activity. Catal Commun 37:55–59
16. Duo FF, Wang YW, Mao XM, Zhang XC, Wang YF, Fan CM (2015) A $BiPO_4$/BiOCl heterojunction photocatalyst with enhanced electron-hole separation and excellent photocatalytic performance. Appl Surf Sci 340:35–42

17. Li ZS, Yang SY, Zhou JM, Li DH, Zhou XF, Ge CY, Fang YP (2014) Novel mesoporous g-C_3N_4 and $BiPO_4$ nanorods hybrid architectures and their enhanced visible-light-driven photocatalytic performances. Chem Eng J 241:344–351
18. Zhang YH, Shen B, Huang HW, He Y, Fei B, Lv FZ (2014) $BiPO_4$/reduced graphene oxide composites photocatalyst with high photocatalytic activity. Appl Surf Sci 319:272–277
19. Chen FJ, Cao YL, Jia DZ (2013) Facile synthesis of Bi_2S_3 hierarchical nanostructure with enhanced photocatalytic activity. J Colloid Interf Sci 404:110–116
20. Zhang ZJ, Wang WZ, Wang L, Sun SM (2012) Enhancement of visible-light photocatalysis by coupling with narrow-band-gap semiconductor: a case study on Bi_2S_3/Bi_2WO_6. ACS Appl Mater Interf 4:593–597
21. Manna G, Bose R, Pradhan N (2014) Photocatalytic Au-Bi_2S_3 heteronanostructures. Angew Chem 126:6861–6864
22. Fang Z, Liu YF, Fan YT, Ni YH, Wei XW, Tang KB, Shen JM, Chen Y (2011) Epitaxial growth of CdS nanoparticle on Bi_2S_3 nanowire and photocatalytic application of the heterostructure. J Phys Chem 115:13968–13976
23. Gao XH, Wu HB, Zheng LX, Zhong YJ, Hu Y, Lou XW (2014) Formation of mesoporous heterostructured $BiVO_4$/Bi_2S_3 hollow discoids with enhanced photoactivity. Angew Chem 126:6027–6031
24. Kim J, Kang M (2012) High photocatalytic hydrogen over the band gap-tuned urchin-like Bi_2S_3-loaded TiO_2 composites system. Int J Hydrogen Energy 37:8249–8256
25. Cui YM, Jia QF, Li HQ, Han JY, Zhu LJ, Li SG, Zou Y, Yang J (2014) Photocatalytic activities of Bi_2S_3/BiOBr nanocomposites synthesized by a facile hydrothermal process. Appl Surf Sci 290:233–239
26. Zhou XF, Lu J, Cao JL, Xu MF, Wang ZS (2014) Simple fabrication of rod-like N-doped TiO_2/Ag with enhanced visible-light photocatalytic activity. Ceram Int 40:3975–3979
27. Liu FZ, Shao X, Li HY, Wang M, Yang SR (2013) Facile fabrication of Bi_2S_3-ZnS nanohybrids on graphene sheets with enhanced electrochemical performances. Mater Lett 108:125–128
28. Wang KX, Shao CL, Li XH, Zhang X, Lu N, Miao FJ, Liu YC (2015) Hierarchical heterostructures of p-type BiOCl nanosheets in electrospun n-type TiO_2 nanofibers with enhanced photocatalytic activity. Catal Commun 67:6–10
29. Chen DM, Kuang Z, Zhu Q, Du Y, Zhu HL (2015) Synthesis and characterization of CdS/$BiPO_4$ heterojunction photocatalyst. Mater Res Bull 66:262–267
30. Li L, Zhang XL, Zhang WZ, Wang LL, Chen X, Gao Y (2014) Microwave-assisted synthesis of nanocomposite Ag/ZnO-TiO_2 and photocatalytic degradation Rhodamine B with different modes. Colloid Surface A 457:134–141
31. Fakhri H, Mahjoub AR, Cheshme Khavar AH (2014) Synthesis and characterization of ZnO/$CuInS_2$ nanocomposite and investigation of their photocatalytic properties under visible light irradiation. Appl Surf Sci 318:65–73
32. Fulekar MH, Singh A, Dutta DP, Roy M, Ballal A, Tyagi AK (2015) Ag incorporated nano $BiPO_4$: sonochemical synthesis, characterization and improved visible light photocatalytic properties. RSC Adv 5:43854–43862
33. Wang WJ, Cheng HF, Huang BB, Lin XJ, Qin XY, Zhang XY, Dai Y (2013) Synthesis of $Bi_2O_2CO_3$/Bi_2S_3 hierarchical microspheres with heterojunctions and their enhanced visible light-driven photocatalytic degradation of dye pollutants. J Colloid Interf Sci 402:34–39
34. Cheng HF, Huang BB, Qin XY, Zhang XY, Dai Y (2012) A controlled anion exchange strategy to synthesize Bi_2S_3 nanocrystals/BiOCl hybrid architectures with efficient visible light photoactivity. Chem Commun 48:97–99
35. Liu XL, Wang WJ, Liu YY, Huang BB, Dai Y, Qin XY, Zhang XY (2015) In situ synthesis of Bi_2S_3/Bi_2SiO_5 heterojunction photocatalysts with enhanced visible light photocatalytic activity. RSC Adv 5:55957–55963
36. Wu ZD, Chen LL, Xing CS, Jiang DL, Xie JM, Chen M (2013) Controlled synthesis of Bi_2S_3/ZnS microspheres by an in situ ion-exchange process with enhanced visible light photocatalytic activity. Dalton Trans 42:12980–12988
37. Cao J, Xu BY, Lin HL, Chen SF (2013) Highly improved visible light photocatalytic activity of $BiPO_4$ through fabricating a novel p-n heterojunction BiOI/$BiPO_4$ nanocomposite. Chem Eng J 228:482–488
38. Ye HF, Lin HL, Cao J, Chen SF, Chen Y (2015) Enhanced visible light photocatalytic activity and mechanism of $BiPO_4$ nanorods modified with AgI nanoparticles. J Mol Catal A Chem 397:85–92